OPEN ACCESS

University of Dundee

University of Dundee

Effects of heterogeneous catalysis in porous media on nanofluid-based reactions

Liu, Chunyan; Pan, Mingyang; Zheng, Liancun; Lin, Ping

Effects of heterogeneous catalysis in porous media on nanofluid-based reactions

Chunyan Liu[a], Mingyang Pan[b], Liancun Zheng[a,*], Ping Lin[c]

[a]*School of Mathematics and Physics, University of Science and Technology Beijing, Beijing 100083, China*
[b]*School of Science and Engineering, The Chinese University of Hong Kong, Shenzhen, Guangdong, 518172, China*
[c]*Division of Mathematics, University of Dundee, Dundee DD1 4HN, Scotland, United Kingdom*

Abstract

This paper studies a new type of homogeneous(HOM)-heterogeneous(HET) reactions in Al_2O_3-water-based nanofluid flowing through porous media over a stretching plate. Prior investigators have focused mainly on the catalytic effects on the plate, we model the influence of heterogeneous catalysis in porous media on these reactions. The HET reactions on the surfaces of porous media and plate are both governed by the first-order kinetics, while the HOM reaction in the fluid is given by the isothermal cubic autocatalytic kinetics. In addition, the thermal conductivity of four distinct shapes of nanoparticle, sphere, brick, cylinder, and platelet, is taken into consideration with the Hamilton-Crosser model. The obtained nonlinear differential systems simplified by using similarity transformations are numerically calculated by the bvp4c algorithm. Results demonstrate that the increase of interfacial area of porous media enhances the rate of surface-catalyzed reaction and therefore porous media can greatly shorten the chemical reaction time. Moreover, we find that platelet nanoparticles exhibit the highest convective heat transfer capacity.

Keywords: Surface-catalyzed reaction, Nanofluid, Particle shape, Porous media

---

*Corresponding author.Tel.:+86(10)6233 2002
Email address: liancunzheng@ustb.edu.cn, liancunzheng@163.com (Liancun Zheng)

1. Introduction

Nanofluids have attracted much attention due to their higher thermal conductivity than traditional base fluids with poor heat transfer performance, such as water, ethylene glycol, and oil. The metallic or nonmetallic nano-scale particles with the diameter of 1-100 nm added base fluids are called as a nanofluid which is firstly proposed by Choi [1]. Later on, nanofluids technology is studied by many investigators experimentally and computationally to achieve enhanced heat transfer rates in industry [2–5]. Bachok et al. [6] reported that flow and heat transfer features of nanofluids on a moving plate containing different types of nanoparticles: Cu, Al_2O_3 and TiO_2. Lin et al. [7] investigated particle shape effects on the Marangoni boundary layer flow in a copper-water nanofluid. The influence of nanoparticle shape on nanofluid forced convection in porous media is examined by Sheikholeslami and Bhatti [8]. In this paper, we consider the influence of the shape and volume fraction of Al_2O_3 nanoparticles in porous media on the velocity, temperature and concentration fields.

Porous media is a material containing many tiny pores, which is widely used in industrial production about artificial porous media, such as filters in filter equipment, catalyzer. The flow in porous media has been studied both experimentally and theoretically. Recent examples can be found in catalytic reactive flows in porous media. Hunt et al. [9–11] studied the advective-diffusive transport phenomena in a porous, catalytic microreactor. Further, Guthrie et al. [12, 13] considered the first-order catalytic reaction on the inner surface of parallel-plate microchannel. They used the local thermal non-equilibrium method with two porous-fluid interface models to study the heat transfer in the porous section of the microreactor. At the same time, the heat and mass transfer in a porous microreactor with Casson fluid and inclined magnetic field were presented by Saeed et al. [14, 15]. Importantly, Alizadeh et al. [16] depicted the forced convection of heat and mass on a cylindrical catalytic surface with non-uniform transpiration and impinging flow in porous media. In addition, Gomari et al. [17] reported the nanofluid stagnation-point flows over a cylinder

2

embedded in porous media.

The study of HOM-HET reactions has numerous important engineering applications such as combustion, catalysis, biochemical systems. Chaudhary et al. [18–20] studied a simple model for HOM-HET reactions in boundary layer flow. Later, Khan and Pop [21] described the effects of suction and injection on the stagnation-point flow over an infinite permeable wall with HOM-HET reactions. Further, Bachok et al. [22] investigated the stretching sheet with HOM-HET reactions effects. Kameswaran et al. [23] presented the HOM-HET reactions in a nanofluid flow by a porous stretching sheet. Qayyum [24] considered the HOM-HET reactions in the MHD mixed convective flow. The isothermal HOM reaction represented by cubic autocatalysis in the flow field is defined as [20]:

$$A + 2B \rightarrow 3B, \tag{1}$$

and HET reaction on the catalyst surface by a first-order process is defined as:

$$A \rightarrow B, \tag{2}$$

where A and B are chemical species having concentrations a and b, respectively. For HOM reaction, the reaction rate is given by

$$\frac{\partial a}{\partial t} = \frac{\partial b}{\partial t} = -k_c ab^2. \tag{3}$$

The reaction rate of the first order reaction occurring at the fluid-solid interface is as follows:

$$D_A \frac{\partial a}{\partial n} = -D_B \frac{\partial b}{\partial n} = k_s a, \tag{4}$$

where D_A and D_B are the diffusion coefficients of species A and B, respectively. n is the unit normal vector towards the fluid and k_s is the HET reaction rate constant. In the above studies, scholars considered that species A reacts heterogeneously on the wall (catalyst surface). That is to say, the wall's surface or the wall itself is a catalyst. In our paper, porous media and stretching surface consist of the same catalyst. In this way, the HET reaction also occurs on the surface of porous media, called surface-catalyzed reaction. The reaction rate in

porous media is governed by [25]

$$r_p = -S k_s a, \tag{5}$$

where S is the interfacial area of the porous media.

The structure of the paper is as follows: in Section 2, the mathematical formulations of the model are proposed. The analyses of numerical results and discussions are studied in Section 3. The conclusions have been summarized in Section 4.

2. Formulation of the problem

Al_2O_3-water nanofluid is adopted as the working fluid past a stretching sheet in porous media consisting of the catalyst shown in Fig. 1. The influence of nanoparticles with different shapes on heat transfer is considered. The subsequent analysis includes the following assumptions [9].

- The nanofluid flow is a two-dimensional steady laminar flow, which satisfies the condition of no-slip boundary.

- The HET reactions on the surfaces of porous media and plate are both governed by the first-order kinetics, while the HOM reaction in the fluid is given by the isothermal cubic autocatalytic kinetics.

- The diffusion coefficients of chemical species A and B are of comparable size.

- The thermal dispersion, thermal radiation and local thermal non-equilibrium in porous media are ignored.

- The porous media is homogenous and isotropic, and the chemical reactions are temperature independent.

- Physical properties such as density, porosity, specific heat, and thermal conductivities are constant.

4

- Velocity of linear stretching sheet along the x-direction is $u_w = cx$, $(c > 0)$.

Based on the above assumptions, the governing equations of flow and heat transfer of a nanofluid with HOM-HET reactions as well as a surface-catalyzed reaction occurring on the surface of porous media can be demonstrated as:

$$\nabla \cdot \mathbf{u} = 0, \tag{6}$$

$$(\mathbf{u} \cdot \nabla)\mathbf{u} = \frac{\mu_{nf}}{\rho_{nf}}\nabla^2\mathbf{u} - \frac{\mu_{nf}}{k\rho_{nf}}\mathbf{u}, \tag{7}$$

$$(\mathbf{u} \cdot \nabla)T = \nabla \cdot (\alpha_{nf}\nabla T), \tag{8}$$

where the velocity vector $\mathbf{u}$ has components (u, v) along the (x, y) axes, k is the permeability of the porous media and $\alpha_{nf} = k_{nf}/(\rho c_p)_{nf}$ is the thermal diffusivity.
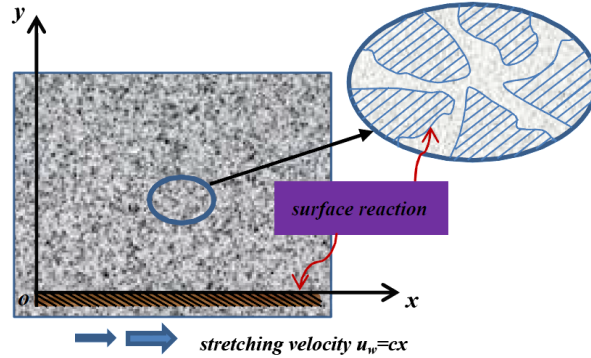

Fig. 1: Schematic diagram.

The equation representing concentration is written in usual notation as:

$$(\mathbf{u} \cdot \nabla)C = \nabla \cdot (D\nabla C), \tag{9}$$

where C shows concentration and D is the mass diffusivity.

Based on Eq. (5), we consider a modified HOM-HET reactions model in the following form:

$$u\frac{\partial a}{\partial x} + v\frac{\partial a}{\partial y} = D_A\frac{\partial^2 a}{\partial y^2} - k_c ab^2 - Sk_s a, \tag{10}$$

5

$$u\frac{\partial b}{\partial x} + v\frac{\partial b}{\partial y} = D_B\frac{\partial^2 b}{\partial y^2} + k_c ab^2 + Sk_s a. \tag{11}$$

The boundary conditions for the momentum, energy and concentration equations are given by

$$\begin{aligned} u = u_w = cx, v = 0, T = T_w, D_A\frac{\partial a}{\partial y} = k_s a, D_B\frac{\partial b}{\partial y} = -k_s a \quad as \quad y = 0 \\ u = 0, T = T_\infty, a = a_0, b = 0 \quad as \quad y \to \infty \end{aligned} \tag{12}$$

where c is the stretching rate and a_0 is uniform concentration of species A.

The effective dynamic viscosity of the nanofluid is given by Brinkman model [26]:

$$\mu_{nf} = \frac{\mu_f}{(1-\phi)^{2.5}}, \tag{13}$$

where ϕ is the volume fraction of nanoparticles and μ_f indicates the dynamic viscosity of fluid. The nanofluid density based on nanoparticles volume fraction is used [27]:

$$\rho_{nf} = \rho_f(1-\phi) + \rho_p\phi, \tag{14}$$

in which ρ_f is the density of fluid and ρ_p is the density of nano-solid-particles. The properties of nanofluid are depicted in Table 1.

Table 1: Physical properties of nanoparticles and base fluid (water).

	Properties				
	ρ_p [kg m^{-3}]	c_p [J kg^{-1}K^{-1}]	k [W m^{-1}K^{-1}]	β [K^{-1}]	σ [Ω^{-1}m^{-1}]
(Al$_2$O$_3$)	3970	765	40	0.85×10^{-5}	1×10^{-10}
(H$_2$O)	997.1	4179	0.613	21×10^{-5}	0.05

The effects of nanoparticle shapes on thermal conductivity of the Al$_2$O$_3$-water nanofluid are studied by Hamilton-Crosser model [28]:

$$\frac{k_{nf}}{k_f} = \frac{k_p + (m-1)k_f - (m-1)\phi(k_f - k_p)}{k_p + (m-1)k_f + \phi(k_f - k_p)}, \tag{15}$$

where k_p and k_f are the conductivities of the particle material and the base fluid, m is shape factor. For different nanoparticle shapes, the values of sphericity are given in Table 2.

Table 2: The values of sphericity and shape factor of different shapes of nanoparticles [28, 29].

Nanoparticle shapes		Aspect ratio	Sphericity φ	Shape factor m
Sphere		-	1	3
Platelet		1:1/8	0.52	5.7
Cylinder		1:8	0.62	4.9
Brick		1:1:1	0.81	3.7

Introducing the following dimensionless variables

$$\eta = \left(\frac{c}{\nu_f}\right)^{1/2} y, \psi = (c\nu_f)^{1/2} x f(\eta), \theta(\eta) = \frac{T - T_\infty}{T_w - T_\infty}, g(\eta) = \frac{a}{a_0}, h(\eta) = \frac{b}{a_0}, \quad (16)$$

and substituting Eq. (16) into Eqs. (6)-(8) and Eqs. (10)-(12), then we obtain

$$f''' + \phi_1 f f'' - \phi_1 f'^2 - k_1 f' = 0, \tag{17}$$

$$\phi_2 \theta'' + \Pr f \theta' = 0, \tag{18}$$

$$\frac{1}{Sc} g'' + f g' - K_c g h^2 - K_{vs} g = 0, \tag{19}$$

$$\frac{\delta}{Sc} h'' + f h' + K_c g h^2 + K_{vs} g = 0. \tag{20}$$

The corresponding dimensionless boundary conditions are

$$\begin{cases} f(0) = 0, f'(0) = 1, f'(\eta) \to 0 \quad as \quad \eta \to \infty \\ \theta(0) = 1, \theta(\eta) \to 0, \quad as \quad \eta \to \infty \\ g'(0) = K_s g(0), g(\eta) \to 1 \quad as \quad \eta \to \infty \\ \delta h'(0) = -K_s g(0), h(\eta) \to 0 \quad as \quad \eta \to \infty \end{cases}, \tag{21}$$

7

where

$$\phi_1 = (1 - \phi)^{2.5} \left[(1 - \phi) + \phi \frac{\rho_p}{\rho_f} \right], \phi_2 = \frac{k_{nf}}{k_f} \frac{1}{\left((1 - \phi) + \phi \frac{(\rho c_p)_p}{(\rho c_p)_f} \right)}. \qquad (22)$$

The primes denote derivative with respect to η. The dimensionless constants in Eqs. (17)-(21) are the permeability parameter k_1, the Prandtl number Pr, the Schmidt number Sc, the HOM parameter K_c, the HET parameter K_s, the surface-catalyzed parameter K_{vs}, and the ratio of the diffusion coefficient δ. They are respectively defined as:

$$k_1 = \frac{\mu_f}{\rho_f k_c}, Pr = \frac{\nu_f}{\alpha_f}, Sc = \frac{\nu_f}{D_A}, K_c = \frac{k_c a_0^2}{c},$$

$$K_{vs} = S_v K_s, S_v = \frac{S D_A}{c^{1/2} \nu_f^{1/2}}, K_s = \frac{k_s \nu_f^{1/2}}{D_A c^{1/2}}, \delta = \frac{D_B}{D_A}, \qquad (23)$$

where S_v is interfacial area parameter. Under the assumption that the diffusion coefficients $D_A = D_B$, i.e., $\delta = 1$ [18], we have from Eqs. (19) and (20)

$$g(\eta) + h(\eta) = 1. \qquad (24)$$

Thus Eqs. (19) and (20) reduce to

$$\frac{1}{Sc} g'' + fg' - K_c g(1 - g)^2 - K_{vs} g = 0, \qquad (25)$$

and are subject to the boundary conditions

$$g'(0) = K_s g(0), g(\eta) \to 1 \quad as \quad \eta \to \infty. \qquad (26)$$

The local Nusselt number is

$$Nu_x = \frac{x q_w}{k_f (T_w - T_\infty)}, q_w = -k_{nf} \frac{\partial T}{\partial y} \bigg|_{y=0} \implies Nu_x = -\frac{k_{nf}}{k_f} \theta'(0) \sqrt{Re_x}, \qquad (27)$$

where $Re_x = u_w x / \nu_f$ shows the local Reynolds number.

3. Results and Discussions

In this paper, we study the effects of modified HOM-HET reactions on the flow of Al_2O_3-water nanofluid over a stretching plate through porous media.

It is noteworthy that the porous media and the surface of the stretching plate consist of the same catalyst. So the surface-catalyzed reaction takes place on the surface of porous media. The effects of Al_2O_3 nanoparticles with different shapes on heat transfer are also considered. The set of coupled nonlinear ordinary differential equations (17)-(18) and (25) subjected to the boundary conditions given in Eq. (26) are solved by using bvp4c with surface-catalyzed parameter K_{vs}, Schmidt number Sc, HOM parameter K_c, HET parameter K_s, Prandtl number Pr, volume fraction of nanoparticles ϕ and shape factor m as prescribed parameters.

3.1. Validation

In order to verify the model, relevant parameters are set to make the physical problem similar to the problem that has been studied in the literature. In particular, the volume fraction of nanoparticles is reduced to zero and the catalytic layer is discarded. Table 3 shows that the numerical results $-f''(0)$ obtained are compared with the analytical and numerical results obtained by predecessors [23, 30] for different permeability parameter k_1. It is seen that the present results are in excellent agreement with both results presented by Kameswaran et al. [23] and Hayat et al. [30].

Table 3: Comparison between values of $-f''(0)$ and previous results for different k_1.

k_1	Kameswaran et al. [23]		Hayat et al. [30]	Present work
	Analytical	Numerical	Numerical	Numerical
1	1.41421356	1.41421356	1.4142	1.4142
1.5	1.58113883	1.58113883	1.5811	1.5811
2	1.73205081	1.73205081	1.7320	1.7321
5	2.44948974	2.44948974	2.4494	2.4495

3.2. Temperature fields

Fig. 2 shows the dimensionless temperature distribution curves with varying Prandtl number Pr. The temperature distributions decrease with the increase

of Prandtl number. Physically, the increase of Prandtl number decreases the thermal diffusivity of the Al_2O_3-water nanofluid. The thickness of the thermal boundary layer is also reduced. Conversely, the temperature is higher in view of the higher permeability parameter. It has been proved that decreasing the permeability of porous media increases the Nusselt number [12, 31], which leads to a decrease in the temperature of Al_2O_3-water nanofluids.
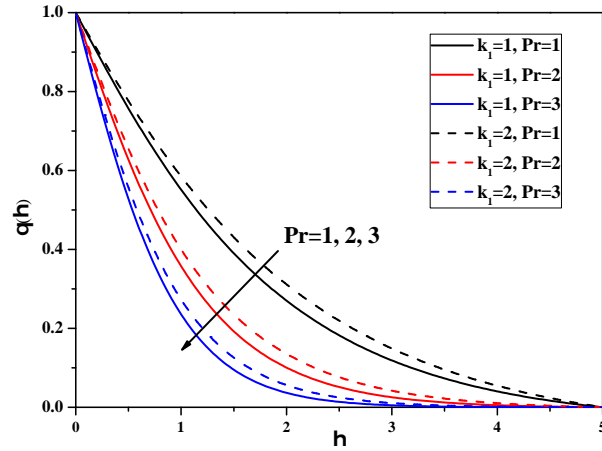

Fig. 2: Temperature distribution curves for parameters $\phi = 0.01, m = 5.7, Sc = 1, K_s = 1, K_{vs} = 1$ and $K_c = 1$ with different values of Prandtl number Pr.

The influence of volume fraction of Al_2O_3 nanoparticles on temperature distribution curves is indicated in Fig. 3. When the shape of nanoparticles is fixed, the temperature goes up due to the increase of volume fraction of nanoparticles ϕ. With the enhancement of volume fraction of nanoparticles, the thermal conductivity and the thickness of the thermal boundary layer increase, which is in line with the main purpose of using nanofluids. It is worth noting that when the volume fraction of nanoparticles is small($\phi = 0.01$), no matter how the shape of nanoparticles changes, the temperature will not be affected. As can be seen from Fig. 3, when the volume fraction is large and fixed, the temperature of platelet-type nanoparticles is higher than that of sphere.
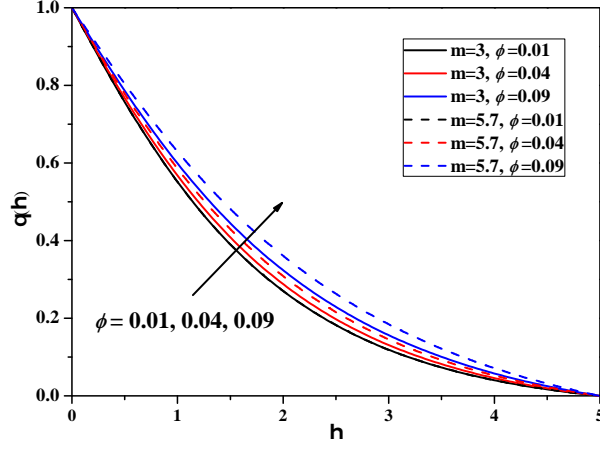
10

Fig. 3: Temperature distribution curves for parameters $Pr = 1, Sc = 1, K_s = 1, K_{vs} = 1, K_c = 1$ and $k_1 = 1$ with different values of volume fraction of nanoparticles ϕ.

3.3. Ratio of thermal conductivity and Nusselt number

Linear regression is carried out with the volume fraction of nanoparticles and the ratio of thermal conductivity, as shown in Fig. 4. Fig. 4 illustrates the influence of different shapes of nanoparticles (Sphere, Brick, Cylinder, and Platelet) on the heat characteristics of Al_2O_3-water nanofluid about the ratio of thermal conductivity k_{nf}/k_f. The ratio of thermal conductivity increases linearly with the elevated volume fraction of nanoparticles. The ratio of thermal conductivity is improved in turn: spheres, bricks, cylinders, and platelets from the slopes of Fig. 4. Similarly, the local Nusselt number is an increasing function of the volume fraction of nanoparticles in Fig. 5. Previously, the analytical results of nanofluid flow in porous catalytic microreactors have been reported [9]. The regression results have well goodness of fit R^2. There is a positive correlation between local Nusselt number and shape factor m (Sphere < Brick < Cylinder < Platelet). Local Nusselt number is the ratio of convective heat transfer to conductive heat transfer. In order to enhance convective heat transfer, it is necessary to make Nu_x as large as possible. There is no doubt that platelet nanoparticle, which has the largest slope, should be chosen.
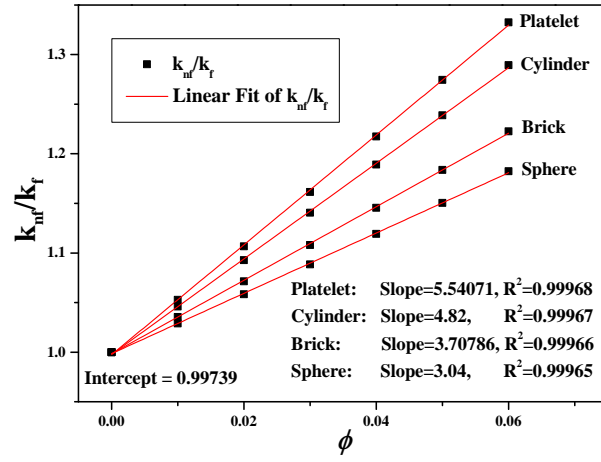
11

Fig. 4: Effects of different nanoparticle shapes on the ratio of thermal conductivity.
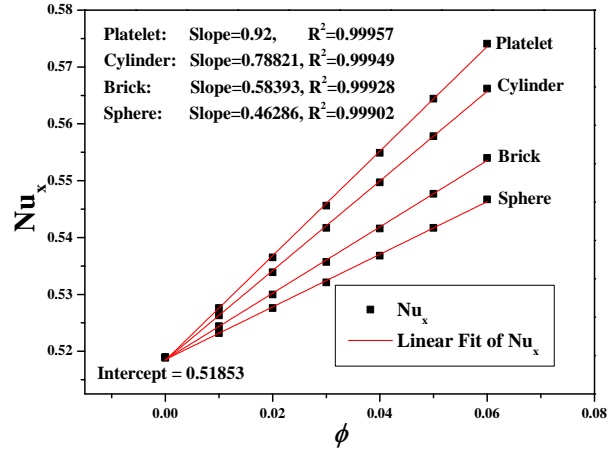

Fig. 5: Effects of different nanoparticle shapes on the local Nusselt number.

3.4. Concentration field

Fig. 6 represents the effects of different values of surface-catalyzed parameter K_{vs} on the dimensionless concentration $g(\eta)$. Results indicate that an enhancement in the surface-catalyzed parameter decreases the concentration. The concentration boundary layer becomes thicker due to the increase of the surface-catalyzed parameter. Physically, the surface-catalyzed reaction rate speeds up with the increase of reaction interface on porous media, and the concentration

of species A gradually reaches the lowest at the same position (η fixed). Compared with the non-catalytic porous media ($k_1 = 1$, $K_{vs} = 0$), the concentration of species A obviously decreases on the porous media and the sheet with the same catalyst when η is fixed. This indicates that the porous media composed of the same catalyst as the sheet greatly shortens the reaction time. It is noted that when $k_1 = 0$, there are no porous media in the physical model, and the concentration of species A is maximum at the same position.
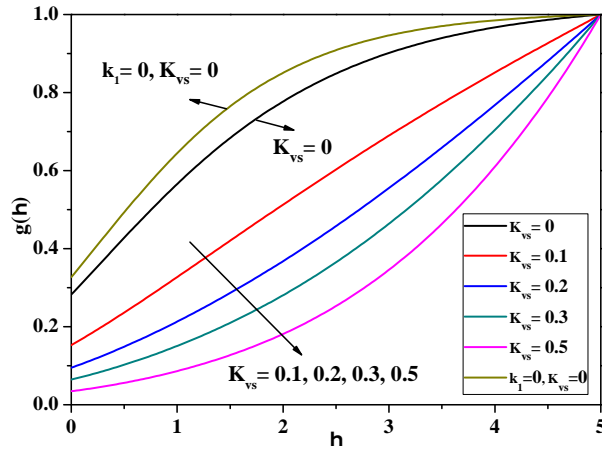

Fig. 6: Concentration distribution curves for parameters $\phi = 0.01, Pr = 1, m = 5.7, Sc = 1, K_s = 1, K_c = 1$ and $k_1 = 1$ with different values of surface-catalyzed parameter K_{vs}.

Fig. 7 demonstrates the impact of Schmidt number Sc on concentration distribution of species A. It is obvious that by enhancing the values of Sc, concentration $g(\eta)$ decreases, while the boundary layer thickness becomes thicker. Sc is prescribed as the ratio of kinematic viscosity to the diffusion coefficient. The velocity diffusion of species A is dominant with an increase of Sc, which causes the reactant particles to accelerate and collide, thus concentration decays. It is also noted that the concentration is high in surface-catalyzed parameter $K_{vs} = 0.5$ case compared to $K_{vs} = 1$ case. This is because when K_{vs} becomes larger, it means that the adsorption interface on porous media becomes wider, resulting in a faster reaction rate.
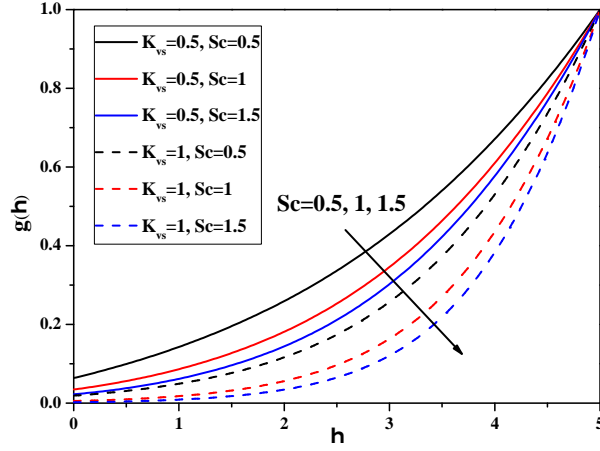
Fig. 7: Concentration distribution curves for parameters $\phi = 0.01, Pr = 1, m = 5.7, K_c = 1, K_s = 1$ and $k_1 = 1$ with different values of Schmidt number Sc.

The variation of dimensionless wall concentration for different values of HOM parameter K_c and HET parameter K_s is shown in Fig. 8. It is observed that concentration at the surface decreases as the strength of the HOM-HET reactions increases. It is worth mentioning that the surface-catalyzed parameter has a great influence on the wall concentration. The intense surface-catalyzed reaction on porous media results in a lower wall concentration.
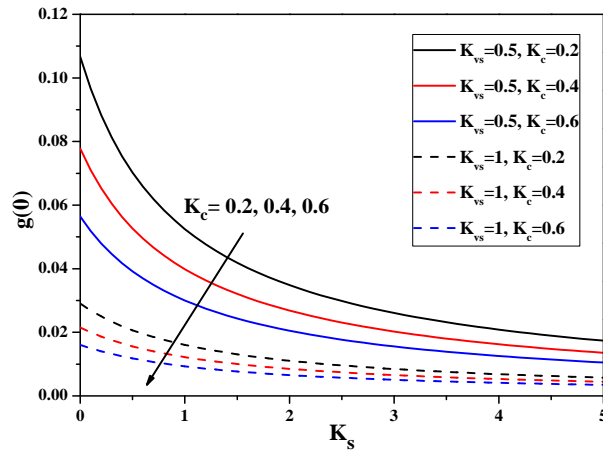

Fig. 8: Wall concentration distribution curves for parameters $\phi = 0.01, Pr = 1, m = 5.7, Sc = 1$ and $k_1 = 1$ with different values of HOM parameter K_c and HET parameter K_s.

14

The influence of HOM parameter K_c on the dimensionless concentration is displayed in Fig. 9. The concentration drops as indicated by the increase in HOM parameter. This is because the increase of the HOM parameter of the same position (η fixed) accelerates the rate of HOM reaction in fluid, so the concentration of species A comes down. Further the concentration distribution in case of surface-catalyzed parameter $K_{vs} = 0.5$ is higher than $K_{vs} = 1$ for $K_c = 0.5, 1, 1.5$. Furthermore, the increase in K_{vs} causes thickening in the concentration boundary layer.
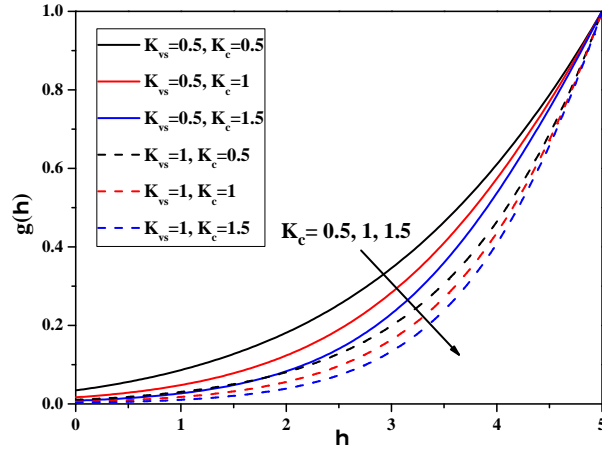

Fig. 9: Concentration distribution curves for parameters $\phi = 0.01, Pr = 1, m = 5.7, Sc = 1, K_s = 1$ and $k_1 = 1$ with different values of HOM parameter K_c.

4. Conclusions

In this article, analysis has been made for the Al_2O_3-water nanofluid with novel HET-HOM reactions in the presence of porous media consisting of the catalyst. The surface-catalyzed reaction occurring on the surface of porous media is considered for the first time in HET-HOM reactions model. The numerical solutions of governing equations are obtained by using bvp4c. The relation of velocity, temperature and concentration fields with involved physical parameters like surface-catalyzed parameter K_{vs}, HOM parameter K_c, HET parameter K_s, Prandtl number Pr, volume fraction of nanoparticles ϕ and Schmidt number Sc

has been discussed. The effects of different nanoparticle shapes on heat transfer properties with Hamilton-Crosser model are also considered. The main results are listed as follows:

- The concentration of chemical species A is a decreasing function of Schmidt number due to the accelerated collision of reactant particles.

- With the influence of heterogeneous catalysis in porous media, the increase of surface-catalyzed parameter leads to a violent reaction on porous media and shortens reaction time.

- Platelet nanoparticles have the highest convective heat transfer capacity in Al_2O_3-water nanofluid and deserve further study.

Acknowledgments

[1] S. U. Choi, J. A. Eastman, Enhancing thermal conductivity of fluids with nanoparticles, Tech. rep., Argonne National Lab., IL (United States) (1995).

[2] R. Prasher, P. Bhattacharya, P. E. Phelan, Thermal conductivity of nanoscale colloidal solutions (nanofluids), Physical review letters 94 (2) (2005) 025901.

[3] M. Sheikholeslami, M. Hatami, D. Ganji, Analytical investigation of MHD nanofluid flow in a semi-porous channel, Powder Technology 246 (2013) 327–336.

[4] Y. Zhang, M. Zhang, Y. Bai, Flow and heat transfer of an Oldroyd-B nanofluid thin film over an unsteady stretching sheet, Journal of Molecular Liquids 220 (2016) 665–670.

[5] C. Ho, C. Chang, W.-M. Yan, P. Amani, A combined numerical and experimental study on the forced convection of Al2O3-water nanofluid in a circular tube, International Journal of Heat and Mass Transfer 120 (2018) 66–75.

[6] N. Bachok, A. Ishak, I. Pop, Flow and heat transfer characteristics on a moving plate in a nanofluid, International Journal of Heat and Mass Transfer 55 (4) (2012) 642–648.

[7] Y. Lin, B. Li, L. Zheng, G. Chen, Particle shape and radiation effects on Marangoni boundary layer flow and heat transfer of copper-water nanofluid driven by an exponential temperature, Powder Technology 301 (2016) 379–386.

[8] M. Sheikholeslami, M. Bhatti, Forced convection of nanofluid in presence of constant magnetic field considering shape effects of nanoparticles, International Journal of Heat and Mass Transfer 111 (2017) 1039–1049.

[9] G. Hunt, N. Karimi, M. Torabi, Two-dimensional analytical investigation of coupled heat and mass transfer and entropy generation in a porous, catalytic microreactor, International Journal of Heat and Mass Transfer 119 (2018) 372–391.

[10] G. Hunt, M. Torabi, L. Govone, N. Karimi, A. Mehdizadeh, Two-dimensional heat and mass transfer and thermodynamic analyses of porous microreactors with soret and thermal radiation effectsan analytical approach, Chemical Engineering and Processing-Process Intensification 126 (2018) 190–205.

[11] G. Hunt, N. Karimi, B. Yadollahi, M. Torabi, The effects of exothermic catalytic reactions upon combined transport of heat and mass in porous microreactors, International Journal of Heat and Mass Transfer 134 (2019) 1227–1249.

[12] D. G. Guthrie, M. Torabi, N. Karimi, Combined heat and mass transfer analyses in catalytic microreactors partially filled with porous material-the influences of nanofluid and different porous-fluid interface models, International Journal of Thermal Sciences 140 (2019) 96–113.

[13] D. G. Guthrie, M. Torabi, N. Karimi, Energetic and entropic analyses of double-diffusive, forced convection heat and mass transfer in microreactors assisted with nanofluid, Journal of Thermal Analysis and Calorimetry 137 (2) (2019) 637–658.

[14] A. Saeed, N. Karimi, G. Hunt, M. Torabi, On the influences of surface heat release and thermal radiation upon transport in catalytic porous microreactorsa novel porous-solid interface model, Chemical Engineering and Processing-Process Intensification 143 (2019) 107602.

[15] A. Saeed, N. Karimi, G. Hunt, M. Torabi, A. Mehdizadeh, Double-diffusive transport and thermodynamic analysis of a magnetic microreactor with non-newtonian biofuel flow, Journal of Thermal Analysis and Calorimetry (2019) 1–25.

[16] R. Alizadeh, N. Karimi, A. Mehdizadeh, A. Nourbakhsh, Analysis of transport from cylindrical surfaces subject to catalytic reactions and non-uniform impinging flows in porous media, Journal of Thermal Analysis and Calorimetry (2019) 1–20.

[17] S. R. Gomari, R. Alizadeh, A. Alizadeh, N. Karimi, Generation of entropy during forced convection of heat in nanofluid stagnation-point flows over a cylinder embedded in porous media, Numerical Heat Transfer, Part A: Applications 75 (10) (2019) 647–673.

[18] M. Chaudhary, J. Merkin, A simple isothermal model for homogeneous-heterogeneous reactions in boundary-layer flow. i equal diffusivities, Fluid dynamics research 16 (6) (1995) 311.

[19] M. Chaudhary, J. Merkin, A simple isothermal model for homogeneous-heterogeneous reactions in boundary-layer flow. ii different diffusivities for reactant and autocatalyst, Fluid dynamics research 16 (6) (1995) 335.

[20] J. Merkin, A model for isothermal homogeneous-heterogeneous reactions in boundary-layer flow, Mathematical and Computer Modelling 24 (8) (1996) 125–136.

[21] W. Khan, I. Pop, Flow near the two-dimensional stagnation-point on an infinite permeable wall with a homogeneous–heterogeneous reaction, Communications in Nonlinear Science and Numerical Simulation 15 (11) (2010) 3435–3443.

[22] N. Bachok, A. Ishak, I. Pop, On the stagnation-point flow towards a stretching sheet with homogeneous–heterogeneous reactions effects, Communications in Nonlinear Science and Numerical Simulation 16 (11) (2011) 4296–4302.

[23] P. Kameswaran, S. Shaw, P. Sibanda, P. Murthy, Homogeneous–heterogeneous reactions in a nanofluid flow due to a porous stretching sheet, International journal of heat and mass transfer 57 (2) (2013) 465–472.

[24] S. Qayyum, R. Khan, H. Habib, Simultaneous effects of melting heat transfer and inclined magnetic field flow of tangent hyperbolic fluid over a nonlinear stretching surface with homogeneous–heterogeneous reactions, International Journal of Mechanical Sciences 133 (2017) 1–10.

[25] C. G. Hill, T. W. Root, Introduction to Chemical Engineering Kinetics and Reactor Design, John Wiley & Sons, 2014.

[26] H. C. Brinkman, The Viscosity of Concentrated Suspensions and Solutions, Journal of Chemical Physics 20 (4) (1952) 571–571.

[27] M. Sheikholeslami, D. D. Ganji, Nanofluid convective heat transfer using semi analytical and numerical approaches: A review, Journal of the Taiwan Institute of Chemical Engineers 65 (2016) 43–77.

[28] E. V. Timofeeva, J. L. Routbort, D. Singh, Particle shape effects on thermophysical properties of alumina nanofluids, Journal of Applied Physics 106 (1) (2009) 014304.

[29] X. Shi, P. Jaryani, A. Amiri, A. Rahimi, E. H. Malekshah, Heat transfer and nanofluid flow of free convection in a quarter cylinder channel considering nanoparticle shape effect, Powder Technology.

[30] T. Hayat, Z. Hussain, A. Alsaedi, S. Asghar, Carbon nanotubes effects in the stagnation point flow towards a nonlinear stretching sheet with variable thickness, Advanced Powder Technology 27 (4) (2016) 1677–1688.

[31] C. Dickson, M. Torabi, N. Karimi, First and second law analyses of nanofluid forced convection in a partially-filled porous channel–the effects of local thermal non-equilibrium and internal heat sources, Applied Thermal Engineering 103 (2016) 459–480.

Nomenclature

a, b	concentration of species A and B respectively, $[kg \ m^{-3}]$
a_0	uniform concentration of species A, $[kg \ m^{-3}]$
c	stretching rate, $[m \ s^{-1}]$
D_A, D_B	diffusion coefficient of species A and B, $[m^2 \ s^{-1}]$
g, h	dimensionless concentration of species A and B, $[-]$
K_c	HOM parameter, $[-]$
K_s	HET parameter, $[-]$
K_{vs}	surface-catalyzed parameter, $[-]$
k	permeability of porous media, $[m^2]$
k_1	permeability parameter, $[-]$
$k_i (i = c, s)$	reaction rate constants, $[-]$
$k_j (j = p, f, nf)$	thermal conductivity, $[WK \ m^{-1}]$
m	shape factor, $[-]$
Nu_x	local Nusselt number, $[-]$
Pr	Prandtl number, $[-]$
q_w	heat flux at the wall, $[W \ m^{-2}]$
Re_x	Reynolds number, $[-]$
S	interfacial area, $[m^2 \ g^{-1}]$
Sc	Schmidt number, $[-]$
T	temperature, $[K]$
u, v	velocity in x,y-axis direction, $[m \ s^{-1}]$
u_w	stretching sheet velocity, $[m \ s^{-1}]$
$\mathbf{u}$	velocity vector, $[m \ s^{-1}]$
x, y	x,y-axis, $[m]$
Greek symbols	
α_{nf}	thermal diffusivity, $[m^2 \ s^{-1}]$
η	similarity variable, $[-]$
ϕ	solid volume fraction of nanoparticles, $[-]$
ψ	stream function, $[m^2 \ s^{-1}]$
$\mu_j (j = f, nf)$	dynamic viscosity of fluid, $[Ns \ m^{-2}]$

ν_f	kinematic viscosity of fluid, $[m^2\ s^{-1}]$
$\rho_j(j = p, f, nf)$	density, $[kg\ m^{-3}]$
δ	ratio of the diffusion coefficient, $[-]$
Subscripts	
w	condition at the surface, $[-]$
∞	ambient condition, $[-]$
f	base fluid, $[-]$
p	nano-solid-particles, $[-]$
nf	nanofluid, $[-]$
Superscript	
$'$	differentiation with respect to η, $[-]$